Formation of magnetic impurities and pair-breaking effect in a superfluid Fermi gas

Y. Ohashi

Faculty of Science and Technology, Keio University, Hiyoshi, Yokohama, 223-8522, Japan and
CREST (JST), 4-1-8 Honcho, Saitama 332-0012, Japan
(Received 10 March 2011; published 10 June 2011)

We theoretically investigate the introduction of magnetic impurities into a superfluid Fermi gas. In the presence of a population imbalance ($N_\uparrow > N_\downarrow$, where N_σ is the number of Fermi atoms with pseudospin $\sigma = \uparrow, \downarrow$), we show that *nonmagnetic* potential scatterers embedded in the system are *magnetized* in the sense that some of the excess spin-$\uparrow$ atoms are localized around them. They destroy the superfluid order parameter around them, as in the case of the magnetic impurity effect discussed in the superconductivity literature. This pair-breaking effect naturally leads to localized excited states below the superfluid excitation gap. To confirm our idea in a simple manner, we consider an attractive Fermi-Hubbard model within the mean-field theory at $T = 0$. We determine consistent superfluid properties around a nonmagnetic impurity, such as the superfluid order parameter, local population imbalance, as well as the single-particle density of states, in the presence of a population imbalance. Since competition between superconductivity and magnetism is one of the most fundamental problems in condensed-matter physics, our results would be useful for the study of this important issue in cold Fermi gases.

I. INTRODUCTION

Magnetic impurity effects have been extensively discussed in the field of metallic superconductivity. Within the Born approximation in terms of magnetic impurity scattering, Abrikosov and Gor'kov (AG) [1] showed that the superconducting phase is completely destroyed by magnetic impurities when the impurity concentration exceeds a critical value. Even below the critical impurity concentration, they showed that magnetic impurities remarkably affect superconducting properties, leading to gapless superconductivity [1,2], where the superconducting order parameter still exists but the Bardeen-Cooper-Schrieffer (BCS) excitation gap is absent. We note that such a pair-breaking effect is absent in the case of nonmagnetic impurities, which is sometimes referred to as Anderson's theorem [3].

Shiba extended AG theory to include multiscattering processes beyond the Born approximation [4]. He clarified that magnetic impurities induce bound states below the BCS excitation gap Δ. Using numerical renormalization group theory, Shiba and co-workers further extended this theory to include the Kondo effect [5,6]. They showed that the transition from the Kondo singlet to the spin doublet of magnetic impurity occurs at $T_K/\Delta \simeq 0.3$, where T_K is the Kondo temperature.

The recently realized superfluid Fermi gases in ^{40}K [7] and ^{6}Li [8–10] have the unique property that one can tune the strength of a pairing interaction by adjusting the threshold energy of a Feshbach resonance. Using this property, we can now study superfluid properties from the weak-coupling BCS regime to the strong-coupling Bose-Einstein condensation (BEC) regime in a unified manner [11–21]. In addition, since a cold Fermi gas system is much cleaner and simpler than metallic superconductors, the former is expected to be a useful quantum simulator for studying various phenomena observed in the latter complicated systems, free from extrinsic effects. For example, the pseudogap phenomenon, which has been extensively studied in high-T_c cuprates [22–27], has also

been recently discussed in the strong-coupling regime of cold Fermi gases [28,29]. Since the latter system is dominated by strong-pairing fluctuations, we can study how the pseudogap is induced by pairing fluctuations in a clear manner [30–32]. Thus, if one could study magnetic impurity effects in superfluid Fermi gases, it would be helpful for further understanding the competition between superconductivity and magnetism, which is one of the most fundamental problems in condensed-matter physics.

In this paper, we theoretically discuss the realization of magnetic impurities in a superfluid Fermi gas. So far, *nonmagnetic* impurities have been realized in Bose gases by using other species of atoms [33] and laser light [34]. In highly polarized normal Fermi gases, it has been observed that the minority component behaves as mobile impurities to form Fermi polarons [35,36]. One difficulty in realizing magnetic impurities in a superfluid Fermi gas is that spins ($\sigma = \uparrow, \downarrow$) in this system are actually not real spins but "pseudospins" describing two atomic hyperfine states. Thus, magnetic impurities must also be "pseudomagnetic" objects acting on these atomic hyperfine states. In this paper, to realize such pseudomagnetic scatterers, we use immobile nonmagnetic impurities as seeds. Although the nonmagnetic impurities do not destroy the superfluid state (Anderson's theorem), the superfluid order parameter may slightly decrease around the impurities, because of the slight suppression of particle density, as schematically shown in Fig. 1(a). In this case, when spin-$\uparrow$ atoms are added to the system, since they cannot form Cooper pairs, they behave like polarized magnetic impurities and destroy the superfluid order parameter around them. Thus, in order to minimize the loss of condensation energy by this pair-breaking effect, as shown in Fig. 1(b), excess spin-$\uparrow$ atoms are expected to be localized around the nonmagnetic impurities, because the superfluid order parameter around the impurities has already been slightly suppressed before the spin-$\uparrow$ doping. The resulting nonmagnetic impurities accompanied by localized spin-$\uparrow$ atoms may be viewed as magnetic impurities.
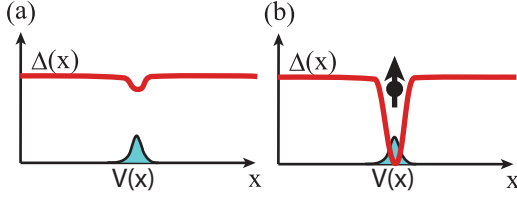
FIG. 1. (Color online) Schematic picture of our idea for realizing magnetic impurities. $V(x)$ is a weak nonmagnetic impurity potential embedded in a superfluid Fermi gas. (a) In an unpolarized Fermi superfluid, although the nonmagnetic impurity does not destroy the superfluid state, the superfluid order parameter $\Delta(x)$ is slightly suppressed around the impurity because of the decrease of particle density by the impurity potential $V(x)$. (b) When a spin-$\uparrow$ atom (solid circle with $\uparrow$) is added to the system, this excess atom is localized around the impurity, so as to minimize the loss of condensation energy by the pair-breaking effect. As a result, the impurity becomes magnetic, and the superfluid order parameter is remarkably suppressed around it.

To confirm this scenario, in this paper we consider a two-dimensional attractive Fermi-Hubbard model with a nonmagnetic impurity. Although this simple lattice model is different from the real three-dimensional continuum Fermi gas system, we emphasize that the presence of a lattice, as well as the low dimensionality, is not essential for the present problem. Within the framework of mean-field theory at $T = 0$, we calculate the spatial variation of the superfluid order parameter, as well as the local population imbalance, around the impurity. In a polarized Fermi superfluid, we confirm that the nonmagnetic impurity is really magnetized. We also show that the superfluid order parameter is damaged by this magnetized impurity, leading to bound states below the BCS excitation gap.

We note that a different method of realizing magnetic impurities has been recently proposed in Ref. [37], where an impurity with $a_\uparrow \neq a_\downarrow$ is used (where a_σ is the scattering length between the impurity and an atom with pseudospin σ). We also note that, under the assumption of the presence of a magnetic impurity, properties of bound states have been examined in Ref. [38].

The outline of this paper is as follows: In Sec. II, we explain our formulation to calculate superfluid properties around a nonmagnetic impurity. In Sec. III, we numerically confirm our idea about the formation of magnetic impurities in a polarized Fermi gas. We discuss bound states induced by the magnetized impurity in Sec. IV. In Sec. V, we briefly examine the effects of a trap potential, as well as finite temperatures. Throughout this paper, we set $\hbar = k_B = 1$ and take the lattice constant to be unity.

II. FORMULATION

We consider a two-component Fermi gas, described by pseudospin $\sigma = \uparrow, \downarrow$. Assuming a two-dimensional square lattice, we put a nonmagnetic impurity at the center of the system. For simplicity, we first ignore the effects of a trap

potential, which will be separately examined in Sec. V. The model Hamiltonian is given by

$$\hat{H} = -t \sum_{\langle i,j \rangle,\sigma} [\hat{c}_{i,\sigma}^\dagger \hat{c}_{j,\sigma} + \text{H.c.}] - U \sum_i \hat{n}_{i,\uparrow} \hat{n}_{i,\downarrow}$$
$$+ \sum_{i,\sigma} [V(i) - \mu_\sigma] \hat{n}_{i,\sigma}, \qquad (1)$$

where $\hat{c}_{i,\sigma}^\dagger$ is the creation operator of a Fermi atom with pseudospin σ at the ith site. $\hat{n}_{i,\sigma} = \hat{c}_{i,\sigma}^\dagger \hat{c}_{i,\sigma}$ is the number operator at the ith site. $-t$ describes atomic hopping between nearest-neighbor sites and the summation $\langle i, j \rangle$ is taken over nearest-neighbor pairs. $-U$ is an on-site pairing interaction between a spin-$\uparrow$ atom and spin-$\downarrow$ atom. Since we consider a polarized Fermi superfluid, the chemical potential μ_σ depends on $\sigma = \uparrow, \downarrow$. The nonmagnetic impurity potential $V(i)$ is assumed to have the form:

$$V(i) = V_0 \frac{\Gamma^2}{(R_x - R_{x0})^2 + (R_y - R_{y0})^2 + \Gamma^2}, \qquad (2)$$

where (R_x, R_y) is the spatial position of the ith lattice site. (R_{x0}, R_{y0}) is the center of the impurity potential.

We treat Eq. (1) within the mean-field theory at $T = 0$. Introducing the superfluid order parameter $\Delta(i) = U \langle \hat{c}_{i,\downarrow} \hat{c}_{i,\uparrow} \rangle$ (which is taken to be real in this paper), as well as the particle density $n_\sigma(i) = \langle \hat{n}_{i,\sigma} \rangle$, we obtain the mean-field Hamiltonian $\hat{H}_{\text{MF}}$ as

$$\hat{H}_{\text{MF}} = -t \sum_{\langle i,j \rangle,\sigma} [\hat{c}_{i,\sigma}^\dagger \hat{c}_{j,\sigma} + \text{H.c.}] - \sum_i \Delta(i)[\hat{c}_{i,\uparrow}^\dagger \hat{c}_{i,\downarrow}^\dagger + \text{H.c.}]$$
$$+ \sum_i [\tilde{V}(i) - \mu] \hat{n}_{i,\sigma} - h \sum_i \hat{s}_{z,i} + \frac{U}{2} \sum_i s_z(i) \hat{s}_{z,i}. \qquad (3)$$

In Eq. (3), we have ignored unimportant constant terms. (We also ignore them in the following discussions.) $\hat{s}_{z,i} = \hat{n}_{i,\uparrow} - n_{i,\downarrow}$ is the spin density operator and

$$s_z(i) = n_\uparrow(i) - n_\downarrow(i) \qquad (4)$$

represents the local magnetization. When this quantity becomes finite around the impurity, the last term in Eq. (3) works as an Ising-type magnetic impurity scatterer. The effective impurity potential $\tilde{V}(i) = V(i) + V_{\text{Hartree}}(i)$ involves the inhomogeneous Hartree term, $V_{\text{Hartree}}(i) = -(U/2)[n_\uparrow(i) - n_\downarrow(i) - n_0]$, where n_0 is the particle density far away from the impurity. $\mu = \mu_{\text{av}} + (U/2)n_0$ is the effective chemical potential, where $\mu_{\text{av}} = [\mu_\uparrow + \mu_\downarrow]/2$. The difference of the spin-dependent chemical potentials,

$$h = \tfrac{1}{2}[\mu_\uparrow - \mu_\downarrow], \qquad (5)$$

works as an effective magnetic field in Eq. (3).

Since Eq. (3) has a bilinear form, we can write it in the form $\hat{H}_{\text{MF}} = \hat{\Phi}^\dagger \tilde{H}_{\text{MF}} \hat{\Phi}$. Here, $\hat{\Phi}^\dagger = (\hat{c}_{1,\uparrow}^\dagger, \hat{c}_{2,\uparrow}^\dagger, \dots, \hat{c}_{M,\uparrow}^\dagger, \hat{c}_{1,\downarrow}, \hat{c}_{2,\downarrow}, \dots, \hat{c}_{M,\downarrow})$, where M is the total number of lattice sites. The Hamiltonian matrix $\tilde{H}_{\text{MF}}$ is chosen so as to reproduce Eq. (3).

As usual, Eq. (3) can be diagonalized by the Bogoliubov transformation,

$$
\hat{\Phi} = \hat{W}
\begin{pmatrix}
\hat{\gamma}_1 \\
\hat{\gamma}_2 \\
\vdots \\
\hat{\gamma}_M \\
\hat{\gamma}_{M+1} \\
\hat{\gamma}_{M+2} \\
\vdots \\
\hat{\gamma}_{2M}
\end{pmatrix}. \tag{6}
$$

The $2M \times 2M$ orthogonal matrix $\hat{W}$ is determined so as to diagonalize $\hat{H}_{\mathrm{MF}}$. The diagonalized mean-field Hamiltonian has the form:

$$
\hat{H}_{\mathrm{MF}} = \sum_{j=1}^{2M} E_j \hat{\gamma}_j^\dagger \hat{\gamma}_j, \tag{7}
$$

where E_j is the jth eigenenergy.

The superfluid order parameter $\Delta(i)$ and the particle density $\langle n_{i,\sigma} \rangle$, are given by, respectively,

$$
\Delta(i) = U \sum_{j=1}^{2M} W_{i,j} W_{M+i,j} \Theta(-E_j), \tag{8}
$$

$$
n_\uparrow(i) = \sum_{j=1}^{2M} W_{i,j}^2 \Theta(-E_j), \tag{9}
$$

$$
n_\downarrow(i) = \sum_{j=1}^{2M} W_{M+i,j}^2 \Theta(E_j), \tag{10}
$$

where $\Theta(x)$ is the step function. The chemical potential μ_σ is determined from the equation for the total number of σ-spin atoms,

$$
N_\sigma = \sum_i n_\sigma(i). \tag{11}
$$

To examine single-particle properties around the impurity, we consider the local density of states (LDOS). To calculate this, we introduce the single-particle thermal Green's function for spin-$\uparrow$ atoms,

$$
G_{\uparrow\uparrow}^{\mathrm{p}}(i,i,i\omega_n) = -\int_0^\beta d\tau e^{i\omega\tau} \langle T_\tau \{\hat{c}_{i,\uparrow}(\tau) \hat{c}_{i,\uparrow}^\dagger(0)\}\rangle, \tag{12}
$$

as well as the Green's function for spin-$\downarrow$ holes,

$$
G_{\downarrow\downarrow}^{\mathrm{h}}(i,i,i\omega_n) = -\int_0^\beta d\tau e^{i\omega\tau} \langle T_\tau \{\hat{c}_{i,\downarrow}^\dagger(\tau) \hat{c}_{i,\downarrow}(0)\}\rangle. \tag{13}
$$

Here, ω_n is the fermion Matsubara frequency and $\beta = 1/T$ is the inverse temperature. In the mean-field theory, Eq. (12) is

given by

$$
\begin{aligned}
G_{\uparrow\uparrow}^{\mathrm{p}}(i,i,i\omega_n) &= -\sum_{j,j'=1}^{2M} W_{i,j} W_{i,j'} \int_0^\beta d\tau e^{i\omega\tau} \langle T_\tau \{\hat{\gamma}_j(\tau) \hat{\gamma}_{j'}^\dagger(0)\}\rangle \\
&= \sum_{j=1}^{2M} \frac{W_{i,j}^2}{i\omega_n - E_j}.
\end{aligned} \tag{14}
$$

Executing the analytic continuation in Eq. (14), we obtain the LDOS for the spin-$\uparrow$ component as

$$
\begin{aligned}
\rho_{i,\uparrow}^{\mathrm{p}}(\omega) &= -\frac{1}{\pi} \mathrm{Im}\big[G_{\uparrow\uparrow}^{\mathrm{p}}(i,i,i\omega_n \to \omega + i\delta)\big] \\
&= \sum_{j=1}^{2M} W_{i,j}^2 \delta(\omega - E_j).
\end{aligned} \tag{15}
$$

In the same manner, the LDOS for the spin-$\downarrow$ component is obtained from the analytic continuation of Eq. (13), as

$$
\begin{aligned}
\rho_{i,\downarrow}^{\mathrm{h}}(\omega) &= -\frac{1}{\pi} \mathrm{Im}\big[G_{\downarrow\downarrow}^{\mathrm{h}}(i,i,i\omega_n \to \omega + i\delta)\big] \\
&= \sum_{j=1}^{2M} W_{M+i,j}^2 \delta(\omega - E_j).
\end{aligned} \tag{16}
$$

In the absence of any nonmagnetic impurity and population imbalance, Eq. (15) reduces to the ordinary superfluid density of states in the uniform BCS state,

$$
\rho_\uparrow^{\mathrm{p}}(\omega) = \sum_{\mathbf{p}} u_{\mathbf{p}}^2 \delta(\omega - E_{\mathbf{p}}) + \sum_{\mathbf{p}} v_{\mathbf{p}}^2 \delta(\omega + E_{\mathbf{p}}), \tag{17}
$$

and Eq. (16) also reduces to the BCS expression,

$$
\rho_\downarrow^{\mathrm{h}}(\omega) = \sum_{\mathbf{p}} u_{\mathbf{p}}^2 \delta(\omega + E_{\mathbf{p}}) + \sum_{\mathbf{p}} v_{\mathbf{p}}^2 \delta(\omega - E_{\mathbf{p}}), \tag{18}
$$

where

$$
u_{\mathbf{p}}^2 = \frac{1}{2}\left[1 + \frac{\xi_{\mathbf{p}}}{E_{\mathbf{p}}}\right], \tag{19}
$$

$$
v_{\mathbf{p}}^2 = \frac{1}{2}\left[1 - \frac{\xi_{\mathbf{p}}}{E_{\mathbf{p}}}\right]. \tag{20}
$$

In Eqs. (19) and (20), $E_{\mathbf{p}} = \sqrt{\xi_{\mathbf{p}}^2 + \Delta^2}$ is the Bogoliubov excitation spectrum, where Δ is the uniform superfluid order parameter. $\xi_{\mathbf{p}} = \varepsilon_{\mathbf{p}} - \mu$ is the kinetic energy $\varepsilon_{\mathbf{p}} = -2t[\cos p_x + \cos p_y]$ of the tight-binding model, measured from the chemical potential μ. As shown in Fig. 2, $\rho_\uparrow^{\mathrm{p}}(\omega)$ and $\rho_\downarrow^{\mathrm{h}}(\omega)$ have BCS coherence peaks at $\omega \simeq \pm 1.8t$, as well as Van Hove singularities associated with the two-dimensional square lattice model at $\omega \simeq \pm 3.2t$. From Eqs. (17) and (18), one finds that $\rho_{i,\uparrow}^{\mathrm{p}}(\omega)$ describes spin-$\uparrow$ particle (hole) excitations when $\omega > 0$ ($\omega < 0$). $\rho_{i,\downarrow}^{\mathrm{h}}(\omega)$ describes spin-$\downarrow$ hole (particle) excitations when $\omega > 0$ ($\omega < 0$).

We note that the physical meaning of $\rho_{i,\uparrow}^{\mathrm{p}}(\omega)$ and $\rho_{i,\downarrow}^{\mathrm{h}}(\omega)$ is slightly altered in the polarized case ($\mu_\uparrow \neq \mu_\downarrow$). In this case, ignoring phase separation phenomenon, we again obtain Eqs. (17) and (18), where the energy ω is replaced by $\omega + h$ [where h is given by Eq. (5)]. Thus, in the polarized case, we need to replace the energy ω by $\omega + h$ in the above discussions about the physical meaning of $\rho_{i,\uparrow}^{\mathrm{p}}(\omega)$ and $\rho_{i,\downarrow}^{\mathrm{h}}(\omega)$.
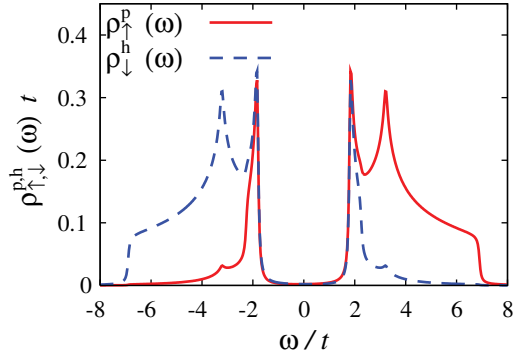
FIG. 2. (Color online) Superfluid density of states in an unpolarized uniform BCS superfluid. The solid line and the dashed line show the spin-↑ component $\rho_\uparrow^p(\omega)$ and the spin-↓ component $\rho_\downarrow^h(\omega)$, respectively. In this figure, we have used the same values for the superfluid order parameter Δ and chemical potential μ, $\Delta(1,1)$ and μ_σ, as in Fig. 5, respectively.

We also note that Eqs. (15) and (16) indicate that $W_{i,j}^2$ and $W_{M+i,j}^2$, respectively, describe the probability densities of spin-↑ and spin-↓ components of the jth eigenstate at the ith site. When we write the wave function of the jth eigenstate in the form $\Psi_j(i) = (\Psi_j^p(i), \Psi_j^h(i))$, where each component is related to $W_{i,j}^2$ and $W_{M+i,j}^2$ as

$$\left|\Psi_j^p(i)\right|^2 = W_{i,j}, \quad \left|\Psi_j^h(i)\right|^2 = W_{M+i,j}, \tag{21}$$

the wave function is normalized as (note that $\hat{W}$ is an orthogonal matrix)

$$\sum_{i=1}^{M} \left[\left|\Psi_j^p(i)\right|^2 + \left|\Psi_j^h(i)\right|^2\right] = \sum_{i=1}^{2M} W_{i,j}^2 = 1. \tag{22}$$

From the physical meaning of $\rho_{i,\uparrow}^p(\omega)$ and $\rho_{i,\downarrow}^h(\omega)$, one may interpret $\Psi_j^p(\omega)$ and $\Psi_j^h(i)$ as the spin-↑ particle and spin-↓ hole components, respectively, when the eigenenergy ω is larger than $-h$. When $\omega < -h$, $\Psi_j^p(\omega)$ and $\Psi_j^h(i)$ have the physical meaning of spin-↑ hole and spin-↓ particle components, respectively. We will use these interpretations in Sec. IV, when we examine the physical properties of bound states.

Before ending this section, we summarize the details of our numerical calculations. We consider a 41×41 square lattice, and impose the periodic boundary condition. For the magnitude of the on-site pairing interaction U, we take $U/t = 6$. To avoid band effects originating from the nested Fermi surface near the half-filling, we consider the low density region, by setting $N_\uparrow = N_\downarrow = 300$ in the absence of a population imbalance (which gives the particle density per lattice site $[N_\uparrow + N_\downarrow]/M = 0.357 \ll 1$). Starting from this unpolarized case, we gradually increase the number of spin-↑ atoms to explore the possibility of a localization of excess atoms around the nonmagnetic impurity at $(R_{x0}, R_{y0}) = (21,21)$. For the impurity potential, we take $V_0/t = 0.25$ and $\Gamma = 1$ in the units of the lattice constant. The resulting impurity potential $V(i = (R_x, R_y))$ is shown in Fig. 3.

Under these conditions, we numerically diagonalize $\tilde{H}_{MF}$ to obtain $\hat{W}$ in Eq. (6), for a given set of $(\Delta(i), n_\uparrow(i),$
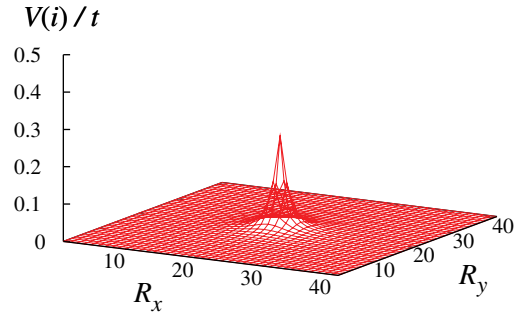

FIG. 3. (Color online) Model nonmagnetic impurity potential $V(i)$ used in this paper. We take $(R_{0x}, R_{0y}) = (21,21)$, $V_0/t = 0.25$, and $\Gamma = 1$.

$n_\downarrow(i), \mu_\uparrow, \mu_\downarrow)$. We update these by using Eqs. (8)–(11) until self-consistency is achieved. We then calculate the superfluid properties around the impurity, such as the LDOSs in Eqs. (15) and (16), as well as the wave functions of low-lying excited states in Eq. (21).

III. FORMATION OF MAGNETIC IMPURITY AND PAIR-BREAKING EFFECT

Figure 4 shows the superfluid properties around the nonmagnetic impurity in the polarized case ($N_\uparrow = 301 > N_\downarrow = 300$). For comparison, we also show the results in the unpolarized case in Fig. 5 ($N_\uparrow = N_\downarrow = 300$). As expected, Figs. 4(a)–4(c) show that the nonmagnetic impurity is *magnetized* in the sense that an excess spin-↑ atom is localized around it. Then, the last term in Eq. (3) works as a magnetic impurity potential. Indeed, Fig. 4(d) shows that the superfluid order parameter $\Delta(i)$ is damaged around the impurity, as in the case of the ordinary magnetic impurity effect in metallic superconductivity [1,4].

In the unpolarized case shown in Fig. 5, such a strong depairing effect is not obtained. The slight decrease of $\Delta(i)$ around the impurity is only seen in Fig. 5(b), reflecting the slight suppression of the particle density $n_\sigma(i)$ shown in Fig. 5(a). This confirms that the remarkable suppression of $\Delta(i)$ in Fig. 4(d) is attributed to, not the original impurity potential $V(i)$, but the localized spin-↑ atom. The role of the weak nonmagnetic impurity potential $V(i)$ is only to slightly decrease the superfluid order parameter around it, so as to capture the excess atom.

When we increase the number of excess spin-↑ atoms, they cluster around the impurity, so that local magnetization $s_z(i)$ around the impurity increases, as shown in Figs. 6(a)–6(c) [39]. In addition, in the case of two excess atoms shown in Fig. 6(b), when we added one more impurity to the system, we obtain two magnetic impurities, as shown in Fig. 6(d), where each impurity is accompanied by one excess spin-↑ atom. Thus, using these one can tune the magnitude of the magnetization of each impurity, as well as the concentration of magnetic impurities.

Here, we comment on the similarity between the magnetization of the nonmagnetic impurity in Fig. 4 and the phase separation observed in polarized Fermi gases [40,41]. In the latter phenomenon, the system spatially separates into an unpolarized superfluid region and a polarized normal
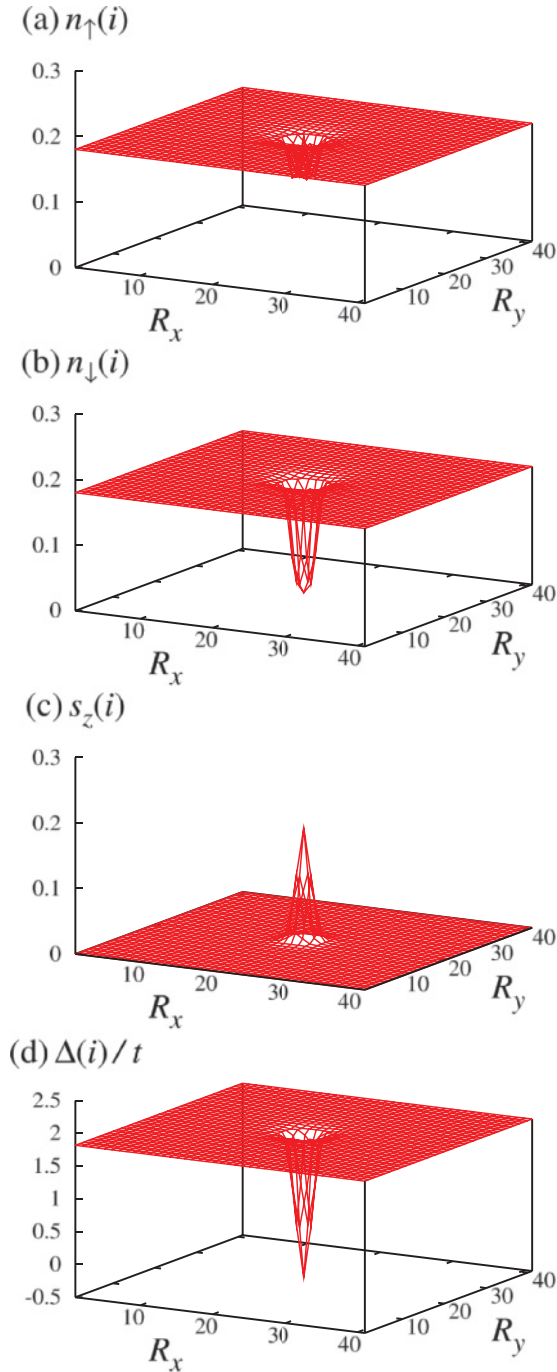
(a) $n_\uparrow(i)$

(b) $n_\downarrow(i)$

(c) $s_z(i)$

(d) $\Delta(i)/t$

FIG. 4. (Color online) Calculated superfluid state around the non-magnetic impurity at $(R_x, R_y) = (21,21)$. We take the population imbalance as $N_\uparrow = 301 > N_\downarrow = 300$, which gives the spin-dependent chemical potentials $\mu_\uparrow = -2.26t$ and $\mu_\downarrow = -5.20t$. Panels (a) and (b) show the particle densities of spin-$\uparrow$ atoms and spin-$\downarrow$ atoms, respectively. (c) Magnetization $s_z(i) = n_\uparrow(i) - n_\downarrow(i)$. (d) Superfluid order parameter $\Delta(i)$. In Fig. 7, we show detailed spatial variations of these quantities around the impurity potential.

region [40–47]. The latter normal region further separates into a partially polarized region and the outer rim of the majority component [36,48]. A similar exclusion of the spin-$\downarrow$ component to the outer rim of the polarized Fermi gas can be seen in the present magnetic impurity problem. Indeed, Fig. 7(a) shows that while the density profile $n_\uparrow(i)$ of spin-$\uparrow$
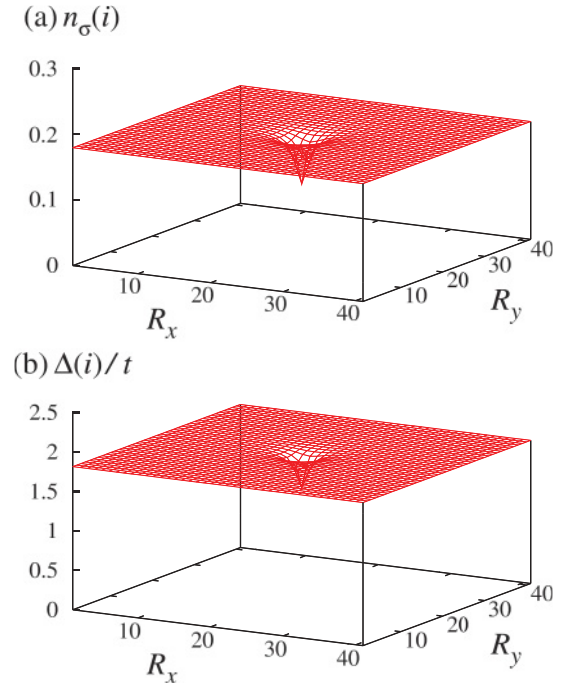
(a) $n_\sigma(i)$

(b) $\Delta(i)/t$

FIG. 5. (Color online) Superfluid state around the nonmagnetic impurity at $(R_x, R_y) = (21,21)$, in the unpolarized case ($N_\uparrow = N_\downarrow = 300$). In this case, we obtain $\mu_\uparrow = \mu_\downarrow = -3.73t$. (a) $n_\sigma(i)$ ($\sigma = \uparrow, \downarrow$). (b) $\Delta(i)$. We note that $s_z(i) = 0$ in the unpolarized case.

atoms is not so different from that in the unpolarized case [except for the enhancement at the impurity site ($R_y = 21$) due to the localization of the excess spin-$\uparrow$ atom], spin-$\downarrow$ atoms are found to be pushed out from the region around the impurity ($R_y \simeq 21$).

(a) $N\uparrow=301$ (b) $N\uparrow=302$
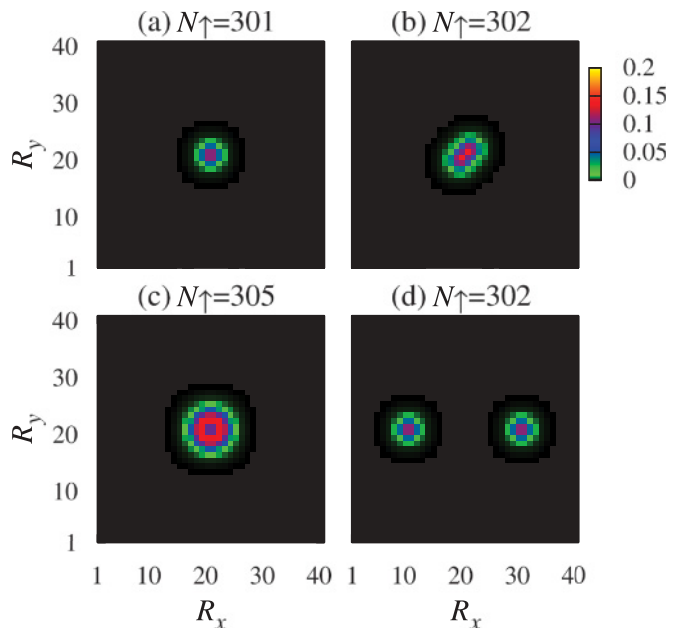
(c) $N\uparrow=305$ (d) $N\uparrow=302$

FIG. 6. (Color online) Intensity of the local magnetization $s_z(i)$ around the impurity at the center of the system. We take $N_\downarrow = 300$. In panel (d), there is an impurity at $(R_x, R_y) = (11,21)$ and at $(31,21)$. The spatial structure of each impurity potential is the same as Eq. (2).
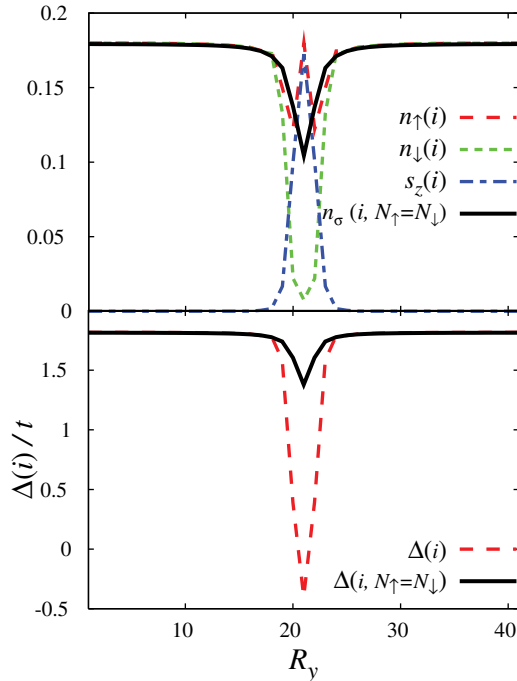
FIG. 7. (Color online) (a) Particle density $n_\sigma(i)$ ($\sigma = \uparrow, \downarrow$) at $R_x = 21$, as a function of R_y. We take $N_\uparrow = 301$ and $N_\downarrow = 300$. In this figure, $n_\sigma(i, N_\uparrow = N_\downarrow)$ is the particle density in the unpolarized case ($N_\uparrow = N_\downarrow = 300$). (b) Spatial variation of the superfluid order parameter $\Delta(i)$ at $R_x = 21$. $\Delta(i, N_\uparrow = N_\downarrow)$ is the result in the absence of a population imbalance ($N_\uparrow = N_\downarrow = 300$).

IV. LOCALIZED EXCITED STATES AROUND THE MAGNETIZED IMPURITY

Figure 8 shows the local density of states (LDOS) $\rho_{i,\uparrow}(\omega)$ around the impurity. In the unpolarized case [panel (a)], the impurity remains nonmagnetic, so that single-particle excitations are almost unaffected by impurity scatterings. The LDOS far away from the impurity (solid line in Fig. 9) agrees with the ordinary BCS density of states $\rho_\uparrow^p(\omega)$ shown in Fig. 2. Even near the impurity, the overall structure of the LDOS is unchanged (see the dashed line in Fig. 9), except for a slightly smaller excitation gap, reflecting the suppression of $\Delta(i)$ around the impurity seen in Fig. 5(b).

The situation is quite different in the presence of a population imbalance. In this case, Fig. 8(b) shows that, in addition to the simple energy shift by the effective magnetic field $h = [\mu_\uparrow - \mu_\downarrow]/2 = -1.47t$, the LDOS is remarkably modified around the impurity. Since the bulk BCS coherence peaks are at $\omega = -3.32t$ and $0.38t$ [see the dashed line in Fig. 10(a)], the four peaks inside the BCS gap ($-3.32t \leqslant \omega \leqslant 0.38t$) around the impurity seen in Fig. 8(b) are found to describe low-lying excited states induced by the magnetized impurity. Since these peaks disappear as one goes away from the impurity, they are bound states localized around the impurity.

These bound states also appear in the spin-$\downarrow$ component of the LDOS $\rho_{i,\downarrow}^h(\omega)$, as shown in Fig. 10(b). The fact that all of the peak positions inside the BCS excitation gap ($-3.32t \leqslant$
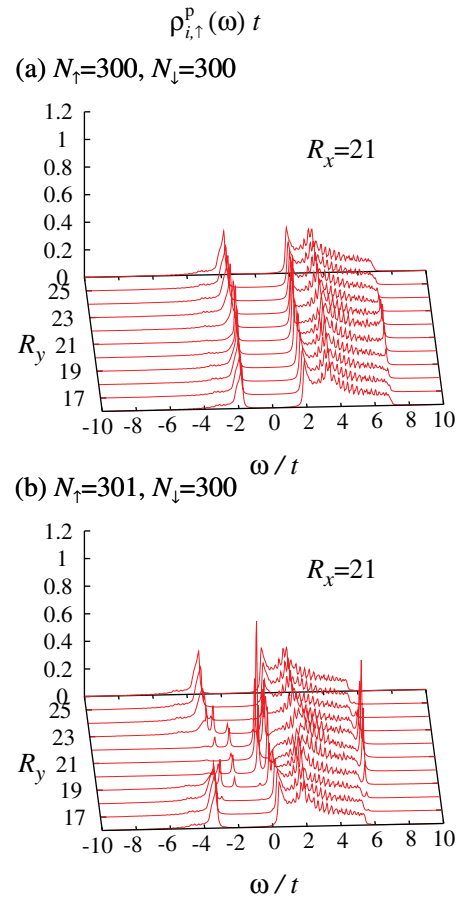

FIG. 8. (Color online) Superfluid local density of states (LDOS) $\rho_{i,\uparrow}^p(\omega)$ around the impurity. In this figure, results at $R_y = 21$ show the LDOS at the impurity site. (a) Unpolarized case ($N_\uparrow = N_\downarrow = 300$). (b) Polarized case ($N_\uparrow = 301 > N_\downarrow = 300$), where one excess spin-$\uparrow$ atom is localized around the impurity. In calculating the LDOS, we have added a small imaginary part $\delta = 0.05t$ to the eigenenergies in order to smear out unphysical fine structures around the coherence peaks, arising from the discrete energy levels in the finite system. We briefly note that the influence of the discrete levels still remains as sharp peaks around the van Hove singularity. We also use this prescription in Figs. 9 and 10.
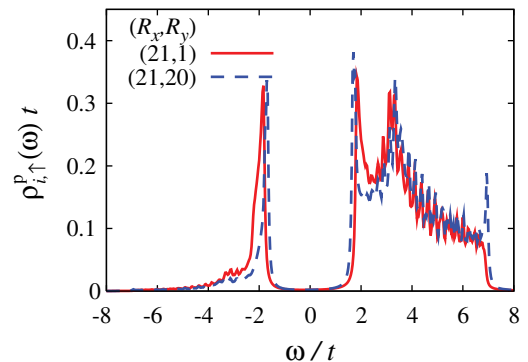

FIG. 9. (Color online) Local density of states $\rho_{i,\uparrow}^p(\omega)$ in the unpolarized case ($N_\uparrow = N_\downarrow = 300$). Apart from the fine peak structure seen around the van Hove singularity (which is due to the discrete levels in the finite system), the LDOS far away from the impurity (solid line) agrees with the uniform BCS density of states $\rho_\uparrow^p(\omega)$ in Fig. 2.
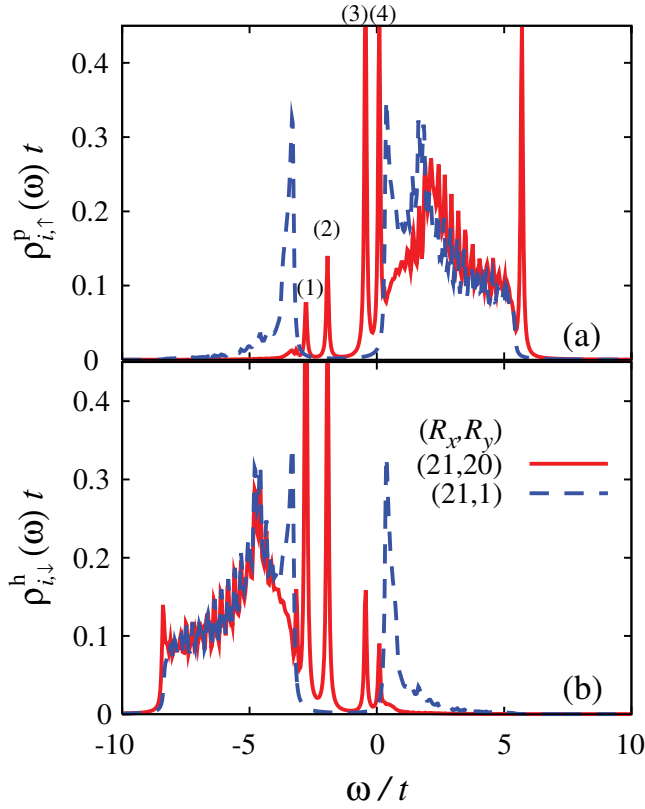
FIG. 10. (Color online) Local density of states in the polarized case ($N_\uparrow = 301 > N_\downarrow = 300$). (a) $\rho_{i,\uparrow}^{\rm p}(\omega)$. (b) $\rho_{i,\downarrow}^{\rm h}(\omega)$. The BCS coherence peaks exist at $\omega = -3.32t$ and $0.38t$ far away from the impurity. [See the dashed lines in panels (a) and (b).]

$\omega \leqslant 0.38t$) are the same in panels (a) and (b) means that they are composite excitations consisting of particle and hole components. To confirm this in a clear manner, for example, we show the wave functions $\Psi_j(i) = (\Psi_j^{\rm p}(i), \Psi_j^{\rm h}(i))$ of the bound states (3) and (4) in Fig. 11.

With regard to the composite character of the localized excited states, we note that the creation operator $\gamma_{\mathbf{p},\uparrow}^\dagger$ of the Bogoliubov excitation in the ordinary uniform BCS state is given by the sum of particle and hole creation operators as

$$\gamma_{\mathbf{p},\uparrow}^\dagger = u_{\mathbf{p}} c_{\mathbf{p},\uparrow}^\dagger + v_{\mathbf{p}} c_{-\mathbf{p},\downarrow}, \qquad (23)$$

where $c_{\mathbf{p},\uparrow}^\dagger$ and $c_{-\mathbf{p},\downarrow}$ are the creation operators of spin-$\uparrow$ particles and spin-$\downarrow$ holes, respectively. That is, this basic property of ordinary single-particle Bogoliubov excitations is found to also hold in the bound states.

As discussed in Sec. II, $\rho_{i,\uparrow}^{\rm p}(\omega)$ and $\rho_{i,\downarrow}^{\rm h}(\omega)$, respectively, describe spin-$\uparrow$ particle (hole) and spin-$\downarrow$ hole (particle) excitations when $\omega > -h$ ($\omega < -h$). Using this, we find that the bound states (1) and (2) in Fig. 10, existing below $-h = -1.47t$, are composed of spin-$\downarrow$ particle and spin-$\uparrow$ hole excitations. Since the energies of the bound states (3) and (4) are larger than $-h = -1.47t$, they are found to be composite excitations of a spin-$\uparrow$ particle and spin-$\downarrow$ hole.

To see the mechanism of bound-state formation, it is helpful to examine the model Hamiltonian in Eq. (3) within the theory of the magnetic impurity effect developed in the field of superconductivity [1,2,4–6], where the spatial variation of the superconducting order parameter is usually ignored. In addition to this simplification, when we also ignore the unimportant nonmagnetic potential $\tilde{V}(i)$ and approximate
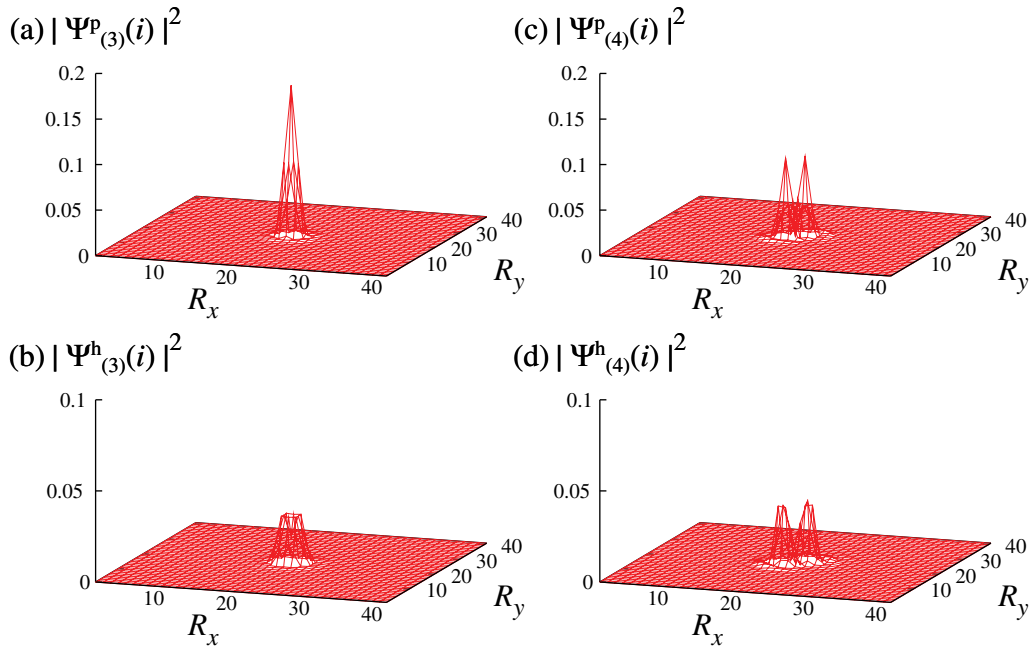

FIG. 11. (Color online) Calculated intensity of the wave functions of bound states. The upper and lower panels show the spin-$\uparrow$ particle and spin-$\downarrow$ hole components, respectively. Panels (a) and (b) show the bound state (3) in Fig. 10. Panels (c) and (d) show the bound state (4). We note that the right panels show one of the two degenerate bound states existing at the peak (4) in Fig. 10. For the other bound state, see Fig. 12(b2).

the magnetic impurity scattering as a δ-functional potential, Eq. (3) reduces to, in momentum space,

$$H = \sum_{\mathbf{p},\sigma}[\xi_{\mathbf{p}} - h\sigma]c_{\mathbf{p},\sigma}^{\dagger}c_{\mathbf{p},\sigma} - \Delta\sum_{\mathbf{p}}[c_{\mathbf{p},\uparrow}^{\dagger}c_{-\mathbf{p},\downarrow}^{\dagger} + \text{H.c.}]$$
$$+ \frac{U}{2}s_z\sum_{\mathbf{p},\mathbf{p}',\sigma}\sigma c_{\mathbf{p},\sigma}^{\dagger}c_{\mathbf{p},\sigma}. \quad (24)$$

Here, s_z is the number of excess spin-↑ atoms localized around the impurity. When s_z can take both positive and negative values depending on the direction of impurity spin, Eq. (24) is just the ordinary Hamiltonian describing classical spin in a superconductor [1,4]. Although the pseudospin in the present case always points in the $+z$ direction (when $N_\uparrow > N_\downarrow$), this difference is not crucial for the bound-state problem. Indeed, Eq. (24) gives the same bound-state solutions as those obtained in the ordinary magnetic impurity problem [4],

$$\omega = -h \pm \Delta\frac{1 - [\pi\rho(0)s_z U/2]^2}{1 + [\pi\rho(0)s_z U/2]^2}, \quad (25)$$

where we have approximated the normal-state density of states to the value $\rho(0)$ at the Fermi level, for simplicity. [For the derivation of Eq. (25), see the Appendix.] While four peaks exist inside the BCS gap in Fig. 10, Eq. (25) only gives two bound states. This means that the spatial variation of the order parameter ignored in Eq. (24) is crucial for the formation of the bound states in the present case.

The superfluid order parameter $\Delta(i)$ is known to be similar to the ordinary potential [49,50]. Thus, the well structure of $\Delta(i)$ shown in Fig. 4(d) makes us expect that the bound states seen in Fig. 10 are trapped by this circular potential well [51]. Indeed, when we examine the bound states with $\omega > -h$, while the wave function of the lowest state (3) in Fig. 10 is almost isotropic and nondegenerate [see Fig. 12(a)], the second lowest states (4) have p-wave symmetry and are doubly degenerate, as shown in Figs. 12(b1) and 12(b2), which is consistent with the well-known result that the angular dependencies of bound states in a circular potential well are given by $\cos(n\theta + \alpha)$ or $\sin(n\theta + \alpha)$ ($n = 0,1,2,\ldots$). In Figs. 12(b1) and 12(b2), one finds $\alpha = \pi/4$, reflecting the breakdown of rotational symmetry by the background square lattice.

We also obtain localized states with higher angular momenta, such as the d-wave ($n = 2$) and f-wave ($n = 3$) states, as shown in the lower four panels of Fig. 12 (although they do not appears as peaks in Fig. 10 [52]). Since their energies are close to the threshold energy $\omega = 0.38t$ of the continuum spectrum, their wave functions spatially spread out, compared with the s-wave bound state in panel (a). Figure 12 indicates that the magnetized impurity would be also useful for the study of a quantum dot in a superfluid Fermi gas.

To show that the well structure of $\Delta(i)$ around the impurity is crucial for bound-state formation in a simple manner, we briefly consider a one-dimensional continuum system and solve a bound-state problem in a pair-potential well $\Delta(x)$,

$$\Delta(x) = \begin{cases} \Delta & (0 \leqslant x \leqslant L), \\ 0 & (x < 0, L < x). \end{cases} \quad (26)$$
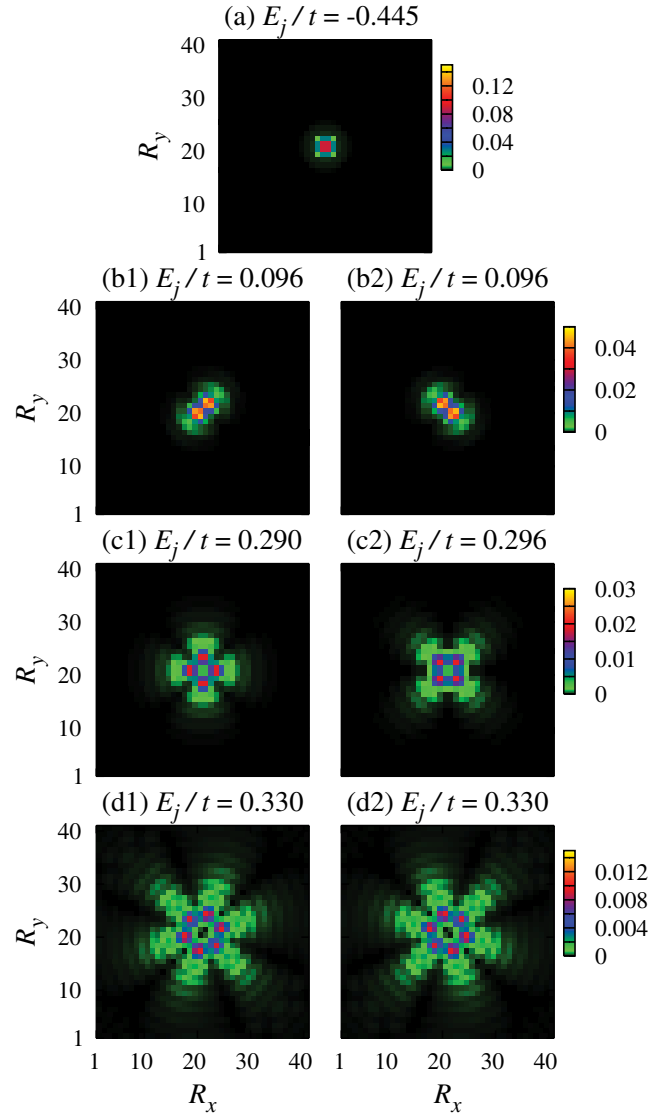

FIG. 12. (Color online) Intensity $|\Psi_j^{\text{p}}(i)|^2$ of the bound-state wave function with $\omega > -h$. Panel (a) shows the wave function of the bound state (3) in Fig. 10. The peak (4) in Fig. 10 consists of doubly degenerate p-wave states given by panels (b1) and (b2). We also show other bound states with higher energies in panels (c) and (d) (although they do not appear as peaks in Fig. 10 [52]). The reason why the degeneracy is lifted in panels (c1) and (c2) is the broken rotational symmetry of the background square lattice.

Solving the Bogoliubov–de Gennes equations under the Andreev approximation [50], we obtain the equation for the bound-state energy E as

$$\frac{\sqrt{\Delta^2 - (E + h_S)^2}}{(E + h_S)} = \tan\left(\sqrt{\frac{m}{2\varepsilon_{\text{F}}}}(E + h_N)L\right), \quad (27)$$

where m is the atomic mass and ε_{F} is the Fermi energy measured from the bottom of the energy band. h_S and h_N describe the effective magnetic fields in the superfluid region ($x < 0$, $L < x$) and the normal-state region ($0 \leqslant x \leqslant L$), respectively. Although we do not explained the detailed derivation of Eq. (27) here, we briefly note that this equation is valid when $E + h_S$ and $E + h_N$ are both
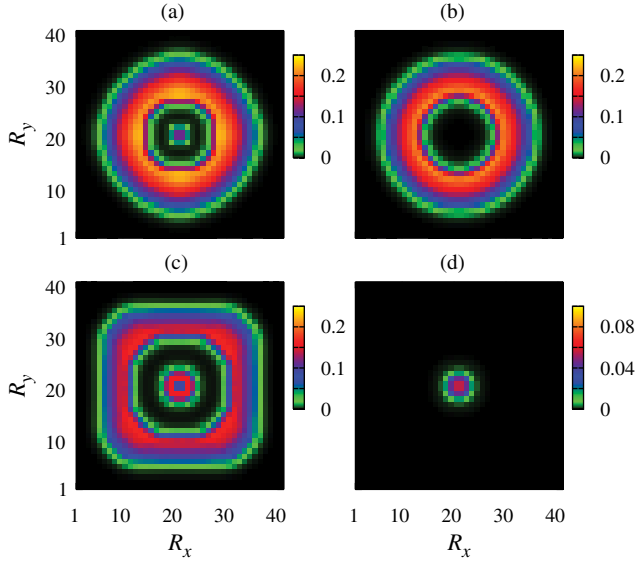
FIG. 13. (Color online) Intensity of local magnetization $s_z(i)$ in a trapped superfluid Fermi gas with a population imbalance. Panels (a) and (b) show the case of the harmonic trap $V_{\text{trap}}^{(2)}(i)$ of Eq. (28). The population imbalance is chosen as (a) $(N_\uparrow, N_\downarrow) = (150, 70)$ and (b) $(N_\uparrow, N_\downarrow) = (150, 80)$. Panel (c) shows the case of the quartic trap $V_{\text{trap}}^{(4)}$ of Eq. (29) with $(N_\uparrow, N_\downarrow) = (150, 80)$. Panel (d) shows the case of the box-type trap $V_{\text{trap}}^{\text{box}}(i)$ of Eq. (30), where we set $(N_\uparrow, N_\downarrow) = (251, 250)$ and $\lambda = 2$. In all the cases, we take $V_{\text{trap}}^0 = 5t$. For the impurity potential at the center of the system, we take $V_0/t = 2$ and $\Gamma = 1$.

positive, which corresponds to the region $\omega > -h$ in Fig. 10. Solving the bound-state equation (27) for the parameter set $(m, \Delta, \varepsilon_F, L, h_S, h_N)$ evaluated in the case of Fig. 10 [53], we obtain the lowest bound-state energy for $\omega > -h$ as $E \simeq -0.45t$, which is consistent with the energy $\omega = -0.445t$ at peak (3) in Fig. 10. Although this is a very simple and rough evaluation, the agreement supports the importance of the well structure of $\Delta(i)$ in the formation of the bound states seen in Fig. 10.

V. EFFECTS OF TRAP POTENTIAL AND FINITE TEMPERATURE

So far, we have ignored the effects of a trap, as well as finite temperatures, for simplicity. In this section, we briefly examine how they affect the localization of excess atoms.

Figure 13(a) shows the intensity of local magnetization $s_z(i)$ in the case when the gas is trapped in the harmonic potential:

$$V_{\text{trap}}^{(2)}(i = (R_x, R_y)) = V_{\text{trap}}^0 \left[\left(\frac{R_x - R_{x0}}{R_{\max} - R_{x0}} \right)^2 + \left(\frac{R_y - R_{y0}}{R_{\max} - R_{y0}} \right)^2 \right]. \quad (28)$$

Here, $(R_{x0}, R_{y0}) = (21, 21)$ is the center of the lattice and $R_{\max} = 41$ is the number of lattice sites in the x and y directions. In this panel, the finite intensity of $s_z(i)$ can be seen around the impurity at $(R_x, R_y) = (21, 21)$, which means that the magnetic-impurity formation discussed in the previous sections also occurs in a trap.
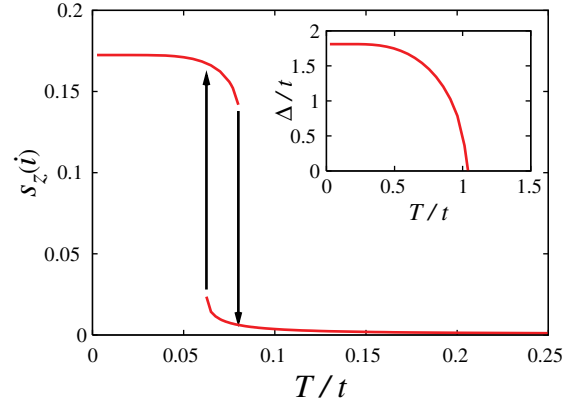

FIG. 14. (Color online) Local magnetization at the impurity site $s_z[i = (21, 21)]$, as a function of temperature. We take $N_\uparrow = 301$ and $N_\downarrow = 300$. The inset shows the calculated superfluid order parameter Δ as a function of temperature in the mean-field theory. In calculating Δ in the inset, we set $N_\uparrow = N_\downarrow = 300$ and ignored the impurity potential.

However, when the population imbalance is lowered, all the excess atoms are localized around the edge of the trap, so that the impurity remains nonmagnetic, as shown in Fig. 13(b). Thus, the population imbalance must be large to some extent to obtain the magnetic impurity.

Since the excess atoms should avoid the spatial region where the potential is very large, the magnetization of the impurity is expected to occur more easily when the trap potential around the edge of the gas is steeper than the harmonic trap in Eq. (28). Indeed, in the case of Fig. 13(b), when we replace the harmonic potential $V_{\text{trap}}^{(2)}(i)$ by a quartic one [54–56],

$$V_{\text{trap}}^{(4)}(i) = V_{\text{trap}}^0 \left[\left(\frac{R_x - R_{x0}}{R_{\max} - R_{x0}} \right)^4 + \left(\frac{R_y - R_{y0}}{R_{\max} - R_{y0}} \right)^4 \right], \quad (29)$$

the localization of excess atoms is realized, as shown in Fig. 13(c). As a more extreme case, when we use the box-type trap [57],

$$V_{\text{trap}}^{\text{box}}(i) = V_{\text{trap}}^0 \left[e^{-(\frac{R_x - 1}{\lambda})^2} + e^{-(\frac{R_x - R_{\max}}{\lambda})^2} + e^{-(\frac{R_y - 1}{\lambda})^2} + e^{-(\frac{R_y - R_{\max}}{\lambda})^2} \right], \quad (30)$$

excess atoms can be localized around the impurity even in the case of a small population imbalance, as shown in Fig. 13(d).

Next we examine the effects of finite temperatures within the mean-field theory [58]. Figure 14 shows the local magnetization $s_z(i)$ at the impurity site, as a function of temperature. We find that the magnetization of the impurity remains finite even at finite temperatures. However, as shown in the inset, the present value of the pairing interaction $U = 6t$ gives the mean-field superfluid phase transition temperature $T_c/t \simeq 1$ in the absence of a population imbalance. Thus, the sudden decrease of $s_z[i = (21, 21)]$ at $T/t \simeq 0.08$ means that the temperature must be far below T_c to realize magnetized impurities.

In Fig. 14, we see the hysteresis of magnetization, which is characteristic of the first-order phase transition. Regarding the present magnetization phenomenon as a kind of phase separation, we find that this hysteresis behavior is consistent

with the phase diagram of a polarized Fermi gas [59,60], where the first-order transition from the phase-separating gas to the superfluid phase occurs far below T_c in the case of a small population imbalance.

VI. SUMMARY

To summarize, we have investigated how to realize magnetic impurities in a superfluid Fermi gas. In a two-dimensional attractive Fermi-Hubbard model, we have calculated the spatial variations of the superfluid order parameter, particle density, as well as polarization, around a nonmagnetic impurity within the framework of the mean-field theory at $T = 0$.

In the presence of a population imbalance ($N_\uparrow > N_\downarrow$), we showed that the nonmagnetic impurity is magnetized in the sense that excess spin-↑ atoms are localized around it. This magnetized impurity behaves like an Ising-type magnetic scatterer, so that the superfluid order parameter is destroyed around it. This pair-breaking effect is similar to the magnetic impurity effect discussed in the superconductivity literature.

Another similarity between the present pseudomagnetic impurity and a real magnetic impurity in a metallic superconductor is that both impurities induce low-lying excited states below the BCS excitation gap. However, while bound-state formation by the latter magnetic impurity is usually discussed when ignoring the spatial variation of the superconducting order parameter, we showed that the local suppression of the superfluid order parameter around the impurity is important in the former case. Namely, bound states are trapped inside a circular potential well formed by the superfluid order parameter. Because of this, the wave function of each bound state behaves like $\cos(n\theta + \alpha)$ or $\sin(n\theta + \alpha)$ ($n = 0, 1, 2, \ldots$) as a function of the angle θ. Thus, this magnetized impurity may also be viewed as a circular quantum dot in a superfluid Fermi gas.

In this paper, we have considered *immobile* impurities. In this regard, mobile impurities have been recently discussed in polarized normal Fermi gases [48,61,62], where Fermi polarons have been observed [35,36]. Mobile impurities have been also investigated in normal [63–65] and superconducting states [66,67] of (unpolarized) metals, where the so-called quantum diffusion phenomenon [68] and effects of the BCS gap on the mobility of impurities [69] have been observed, respectively. Thus, an interesting future problem would be how the mobility of an impurity, the formation of a Fermi polaron, and the quantum diffusion phenomenon affect the formation of the magnetic impurity discussed in this paper.

Since competition between magnetism and superconductivity is one of the most fundamental problems in condensed-matter physics, our results would be useful for the study of this important topic by using superfluid Fermi gases. In this regard, we briefly note that the magnetic impurity discussed in this paper is classical spin, because it does not have an exchange term (which is symbolically written as $s_+\sigma_- + s_+\sigma_-$, where $s_\pm = s_x \pm is_y$ and $\sigma_\pm = \sigma_x \pm i\sigma_y$ represent an impurity spin and the spin of a Fermi atom, respectively). As a result, the Kondo effect is absent. Thus, whilst examining competition between the Kondo singlet and Cooper-pair singlet in cold Fermi gases, an interesting challenge would be to find out how

to realize a quantum magnetic impurity with an exchange term in this system.

APPENDIX: DERIVATION OF THE BOUND-STATE ENERGIES IN EQ. (25)

To discuss the magnetic impurity problem in a Fermi superfluid, it is convenient to introduce the 4×4 matrix thermal Green's function,

$$\hat{G}(\mathbf{p}, \mathbf{p}', i\omega_n) = -\int_0^\beta d\tau e^{i\omega\tau} \langle T_\tau \{\hat{\Psi}_\mathbf{p}(\tau)\hat{\Psi}_{\mathbf{p}'}^\dagger(0)\}\rangle, \quad \text{(A1)}$$

where $\hat{\Psi}_\mathbf{p}^\dagger = (c_{\mathbf{p},\uparrow}^\dagger, c_{\mathbf{p},\downarrow}^\dagger, c_{-\mathbf{p},\downarrow}, c_{-\mathbf{p},\uparrow})$ is the four-component Nambu field [2,4]. In the absence of a magnetic impurity, Eq. (A1) has the form $\hat{G}(\mathbf{p}, \mathbf{p}', i\omega_n) = \delta_{\mathbf{p},\mathbf{p}'}\hat{G}_0(\mathbf{p}, i\omega_n)$, where

$$\hat{G}_0(\mathbf{p}, i\omega_n) = \frac{1}{(i\omega_n + h) - \xi_\mathbf{p}\rho_3 + \Delta\rho_1\tau_3}. \quad \text{(A2)}$$

Here, ρ_i and τ_i ($i = 1, 2, 3$) are Pauli matrices, acting on particle-hole space and spin space, respectively.

The full Green's function in Eq. (A1) is obtained by including all magnetic impurity scatterings, which gives [4]

$$\hat{G}(\mathbf{p}, \mathbf{p}', i\omega_n) = \delta_{\mathbf{p},\mathbf{p}'}\hat{G}_0(\mathbf{p}.i\omega_n)$$
$$+ \hat{G}_0(\mathbf{p}, i\omega_n)\hat{t}(i\omega_n)\hat{G}_0(\mathbf{p}', i\omega_n). \quad \text{(A3)}$$

Here, the t-matrix $\hat{t}(i\omega_n)$ involves the effects of magnetic impurity scatterings as

$$\hat{t}(i\omega_n) = \frac{U}{2}s_z\tau_3 + \left(\frac{U}{2}s_z\right)^2 \tau_3\hat{F}(i\omega_n)$$
$$+ \left(\frac{U}{2}s_z\right)^3 \tau_3\hat{F}(i\omega_n)^2 + \cdots$$
$$= \frac{\frac{U}{2}s_z\tau_3}{1 - \frac{U}{2}s_z\hat{F}(i\omega_n)}, \quad \text{(A4)}$$

where $\hat{F}(i\omega_n) = \sum_\mathbf{k} \hat{G}_0(\mathbf{k}, i\omega_n)\tau_3$. We briefly note that, in the case of the ordinary magnetic impurity problem where the impurity spin is $s_z = \pm s$, we need to take the average over the direction of impurity spin as $\langle s_z^{2n}\rangle = s^{2n}$ and $\langle s_z^{2n+1}\rangle = 0$ ($n = 0, 1, 2, \ldots$). In this case, $\hat{t}(i\omega_n)$ is given by [4]

$$\hat{t}(i\omega_n) = \frac{\left(\frac{U}{2}s\right)^2 \tau_3\hat{F}(i\omega_n)}{1 - \left(\frac{U}{2}s\right)^2 \hat{F}(i\omega_n)^2}. \quad \text{(A5)}$$

As usual, the factor $\hat{F}(i\omega_n)$ in Eq. (A4) can be conveniently evaluated by replacing the momentum summation by energy integration. Assuming the particle-hole symmetry of the fermion band and approximating the normal-state density of states by the value $\rho(0)$ at the Fermi level, one obtains [2,4]

$$F(i\omega_n) = -\pi\rho(0)\frac{(i\omega_n + h)\tau_3 + \Delta\rho_1}{\sqrt{\Delta^2 - (i\omega_n + h)^2}}. \quad \text{(A6)}$$

Bound states are obtained as poles of the analytic continued t-matrix, $\hat{t}(i\omega_n \to \omega + i\delta)$. Using this, we obtain the equation for the bound-state energies as

$$0 = \det\left[1 + \frac{U}{2}\pi s_z \rho(0)\frac{(\omega + h)\tau_3 + \Delta\rho_1}{\sqrt{\Delta^2 - (\omega + h)^2}}\right], \quad (A7)$$

which gives Eq. (25). We briefly note that the bound-state equation in the case of Eq. (A5) is given by

$$0 = \det\left[1 \pm \frac{U}{2}\pi s \rho(0)\frac{(\omega + h)\tau_3 + \Delta\rho_1}{\sqrt{\Delta^2 - (\omega + h)^2}}\right], \quad (A8)$$

which also gives Eq. (25).

[1] A. A. Abrikosov and L. P. Gor'kov, Sov. Phys.—JETP **15**, 752 (1962).

[2] See, for example, K. Maki, in *Superconductivity*, edited by R. D. Parks (Marcel Dekker, New York, 1969), p. 1035.

[3] See, for example, P. G. de Gennes, *Superconductivity of Metals and Alloys* (Addison-Wesley, New York, 1992).

[4] H. Shiba, Prog. Theor. Phys. **40**, 435 (1968).

[5] K. Satori, H. Shiba, O. Sakai, and Y. Shimizu, J. Phys. Soc. Jpn. **61**, 3239 (1992).

[6] O. Sakai, Y. Shimizu, H. Shiba, and K. Satori, J. Phys. Soc. Jpn. **62**, 3181 (1993).

[7] C. A. Regal, M. Greiner, and D. S. Jin, Phys. Rev. Lett. **92**, 040403 (2004).

[8] M. Bartenstein, A. Altmeyer, S. Riedl, S. Jochim, C. Chin, J. H. Denschlag, and R. Grimm, Phys. Rev. Lett. **92**, 120401 (2004).

[9] M. W. Zwierlein, C. A. Stan, C. H. Schunck, S. M. F. Raupach, A. J. Kerman, and W. Ketterle, Phys. Rev. Lett. **92**, 120403 (2004).

[10] J. Kinast, S. L. Hemmer, M. E. Gehm, A. Turlapov, and J. E. Thomas, Phys. Rev. Lett. **92**, 150402 (2004).

[11] For reviews, see Q. Chen, J. Stajic, S. Tan, and K. Levin, Phys. Rep. **412**, 1 (2005); I. Bloch, J. Dalibard, and W. Zwerger, Rev. Mod. Phys. **80**, 885 (2008); S. Giorgini, L. Pitaevskii, and S. Stringari, *ibid.* **80**, 1215 (2008).

[12] D. M. Eagles, Phys. Rev. **186**, 456 (1969).

[13] A. J. Leggett, in *Modern Trends in the Theory of Condensed Matter*, edited by A. Pekalski and J. Przystawa (Springer-Verlag, Berlin, 1980), p. 14.

[14] P. Nozières and S. Schmitt-Rink, J. Low Temp. Phys. **59**, 195 (1985).

[15] C. A. R. Sá de Melo, M. Randeria, and J. R. Engelbrecht, Phys. Rev. Lett. **71**, 3202 (1993).

[16] R. Haussmann, *Self-Consistent Quantum Field Theory and Bosonization for Strongly Correlated Electron Systems* (Springer-Verlag, Berlin, 1999), Chap. 3.

[17] Y. Ohashi and A. Griffin, Phys. Rev. Lett. **89**, 130402 (2002); Phys. Rev. A **67**, 033603 (2003); **67**, 063612 (2003).

[18] A. Perali, P. Pieri, G. C. Strinati, and C. Castellani, Phys. Rev. B **66**, 024510 (2002).

[19] R. Haussmann, W. Rantner, S. Cerrito, and W. Zwerger, Phys. Rev. A **75**, 023610 (2007).

[20] R. Haussmann, and W. Zwerger, Phys. Rev. A **78**, 063602 (2008).

[21] H. Hu, X. J. Liu, and P. D. Drummond, Phys. Rev. A **77**, 061605 (2008).

[22] For reviews, see A. Damascelli, Z. Hussain, and Z. Shen, Rev. Mod. Phys. **75**, 473 (2003); P. A. Lee, N. Nagaosa, and X. Wen, *ibid.* **78**, 17 (2006); O. Fischer, M. Kugler, I. Maggio-Aprile, C. Berthod, and C. Renner, *ibid.* **79**, 353 (2007); Y. Yanase, T. Jujo, T. Nomura, H. Ikeda, T. Hotta, and K. Yamada, Phys. Rep. **387**, 1 (2003).

[23] M. Randeria, N. Trivedi, A. Moreo, and R. T. Scalettar, Phys. Rev. Lett. **69**, 2001 (1992).

[24] J. M. Singer, M. H. Pedersen, T. Schneider, H. Beck, and H.-G. Matuttis, Phys. Rev. B **54**, 1286 (1996).

[25] B. Janko, J. Maly, and K. Levin, Phys. Rev. B **56**, 11407 (1997).

[26] D. Rohe and W. Metzner, Phys. Rev. B **63**, 224509 (2001).

[27] Y. Yanase and K. Yamada, J. Phys. Soc. Jpn. **70**, 1659 (2001).

[28] J. T. Stewart, J. P. Gaebler, and D. S. Jin, Nature (London) **454**, 744 (2008).

[29] J. P. Gaebler, J. T. Stewart, T. E. Drake, D. S. Jin, A. Perali, P. Pieri, and G. C. Strinati, Nature Physics **6**, 569 (2010).

[30] S. Tsuchiya, R. Watanabe, and Y. Ohashi, Phys. Rev. A **80**, 033613 (2009); **82**, 033629 (2010).

[31] R. Watanabe, S. Tsuchiya, and Y. Ohashi, Phys. Rev. A **82**, 043630 (2010).

[32] H. Hu, X.-J. Liu, P. D. Drummond, and H. Dong, Phys. Rev. Lett. **104**, 240407 (2010).

[33] C. Zipkes, S. Palzer, C. Sias, and M. Köhl, Nature (London) **464**, 388 (2010).

[34] G. Modugno, Rep. Prog. Phys. **73**, 102401 (2010).

[35] A. Schirotzek, C. H. Wu, A. Sommer, and M. W. Zwierlein, Phys. Rev. Lett. **102**, 230402 (2009).

[36] S. Nascimbène, N. Navon, K. J. Jiang, L. Tarruell, M. Teichmann, J. McKeever, F. Chevy, and C. Salomon, Phys. Rev. Lett. **103**, 170402 (2009).

[37] E. Vernier, D. Pekker, M. Zwierlein, and E. Demler, Phys. Rev. A **83**, 033619 (2011).

[38] L. Jiang, L. Baksmaty, H. Hu, Y. Chen, and H. Pu, e-print arXiv:1010.3222.

[39] In Fig. 6(b), one sees the anisotropic spatial distribution of excess atoms, which is due to the broken rotational symmetry of the background square lattice.

[40] M. W. Zwierlein, A. Schirotzek, C. H. Schunck, and W. Ketterle, Science **311**, 492 (2006).

[41] G. B. Partridge, W. Li, R. I. Kamar, Y.-A. Liao, and R. G. Hulet, Science **311**, 503 (2006).

[42] T. N. De Silva and E. J. Mueller, Phys. Rev. A **73**, 051602 (2006).

[43] F. Chevy, Phys. Rev. Lett. **96**, 130401 (2006).

[44] P. Pieri and G. C. Strinati, Phys. Rev. Lett. **96**, 150404 (2006).

[45] W. Yi and L.-M. Duan, Phys. Rev. A **73**, 031604 (2006).

[46] T. N. De Silva and E. J. Mueller, Phys. Rev. Lett. **97**, 070402 (2006).

[47] M. Haque and H. T. C. Stoof, Phys. Rev. Lett. **98**, 260406 (2007).

[48] F. Chevy, Phys. Rev. A **74**, 063628 (2006).

[49] P. G. de Gennes, and D. Saint-James, Phys. Lett. **4**, 151 (1963).

[50] J. Demers and A. Griffin, Can. J. Phys. **49**, 285 (1971).

[51] We note that, even in the unpolarized case, the local suppression of the superfluid order parameter shown in Fig. 5(b) may induce bound states. In this case, however, the pair-potential well is shallow as $\Delta(1,1) = 1.81t$ and $\Delta(21,21) = 1.38t$, so that bound states only appear near the BCS gap edges. In the case of Fig. 5, the lowest bound state in the positive energy region appears at $\omega = 1.68t$.

[52] The reason why these bound states cannot be seen in Fig. 10 is that their energies are very close to the BCS gap edge at $\omega = 0.38t$. In addition, since their peaks are broadened by the small imaginary part ($\delta = 0.05t$) added to the eigenenergies whilst calculating the LDOS, they cannot be distinguished from the continuum spectrum above the BCS gap in Fig. 10.

[53] Although the bound-state equation (27) is for a one-dimensional system, we have evaluated the parameter set $(m,\Delta,\varepsilon_{\mathrm{F}},L,h_S,h_N)$ from the self-consistent solution for the two-dimensional case shown in Fig. 4 (where $\mu_\uparrow = -2.26t$ and $\mu_\downarrow = -5.20t$). The resulting values are $m \simeq 1/(2t)$, $\Delta \simeq 1.82t$, $\varepsilon_{\mathrm{F}} \simeq 0.27t$, $L \simeq 2$, $h_S \simeq h = 1.47t$, and $h_N \simeq h - \tilde{s} \simeq 0.96t$. Here, $\tilde{s}$ is the effective molecular field by local magnetization, arising from the last term in Eq. (3). We have evaluated this quantity as $\tilde{s} \simeq (U/2) \times 0.17 = 0.51t$ ($U = 6t$), where 0.17 is the value of the polarization $s_z(i)$ at the center of the impurity potential.

[54] V. Bretin, S. Stock, Y. Seurin, and J. Dalibard, Phys. Rev. Lett. **92**, 050403 (2004).

[55] S. Gautam and D. Angom, Eur. Phys. J. D **46**, 151 (2008).

[56] R. Ramakumar, and A. N. Das, Eur. Phys. J. D **47**, 203 (2008).

[57] T. P. Meyrath, F. Schreck, J. L. Hanssen, C.-S. Chuu, and M. G. Raizen, Phys. Rev. A **71**, 041604 (2005).

[58] At finite temperatures, we replace the step functions $\Theta(-E_j)$ and $\Theta(E_j)$ in Eqs. (8)–(10) by the Fermi distribution functions $f(E_j)$ and $f(-E_j)$, respectively.

[59] Y. Shin, C. H. Schunk, A. Schirotzek, and W. Ketterle, Nature (London) **451**, 689 (2008).

[60] W. Ketterle and M. Zwierlein, in *Ultra-Cold Fermi Gases, Proceedings of the International School of Physics "Enrico Fermi,"* edited by M. Inguscio, W. Ketterle, and C. Salomon (IOS Press, Amsterdam, 2007), p. 95.

[61] N. Prokof'ev and B. Svistunov, Phys. Rev. B **77**, 020408 (2008).

[62] R. Combescot, A. Recati, C. Lobo, and F. Chevy, Phys. Rev. Lett. **98**, 180402 (2007).

[63] J. Kondo, Physica B **125**, 279 (1984).

[64] J. Kondo, Physica B **126**, 377 (1984).

[65] K. Yamada, Prog. Theor. Phys. **72**, 195 (1984).

[66] M. Matsumoto and Y. Ohashi, J. Phys. Soc. Jpn. **62**, 2088 (1993).

[67] Y. Ohashi and M. Matsumoto, J. Phys. Soc. Jpn. **62**, 3532 (1993).

[68] R. Kadono, J. Imazato, T. Matsuzaki, K. Nishiyama, K. Nagamine, T. Yamazaki, D. Richter, and J. M. Welter, Phys. Rev. B **39**, 23 (1989).

[69] R. Kadono, R. F. Kiefl, J. A. Chakhalian, S. R. Dunsiger, B. Hitti, W. A. MacFarlane, J. Major, L. Schimmele, M. Matsumoto, and Y. Ohashi, Phys. Rev. Lett. **79**, 107 (1997).